Elizaveta A. Zamyatina, Sergey Yu. Kottsov, Viktoriia A. Anikina, Anton L. Popov, Marina P. Shevelyova, Nelli R. Popova, Cerium oxide@silica core-shell nanocomposite as multimodal platforms for drug release and synergistic anticancer effects, *Наносистемы: физика, химия, математика*, 2023, том 14, выпуск 5, 560–570

DOI: 10.17586/2220-8054-2023-14-5-560-570

NANOSYSTEMS:
PHYSICS, CHEMISTRY, MATHEMATICS

Zamyatina E.A., Kottsov S.Yu., et al. *Nanosystems: Phys. Chem. Math.*, 2023, **14** (5), 560–570.
http://nanojournal.ifmo.ru
DOI 10.17586/2220-8054-2023-14-5-560-570

Original article

Cerium oxide@silica core-shell nanocomposite as multimodal platforms for drug release and synergistic anticancer effects

Elizaveta A. Zamyatina[1,a], Sergey Yu. Kottsov[2,b], Viktoriia A. Anikina[1,c], Anton L. Popov[1,d], Marina P. Shevelyova[3,e], Nelli R. Popova[1,f]

[1]Institute of Theoretical and Experimental Biophysics of the Russian Academy of Sciences, Pushchino, Russia
[2]Kurnakov Institute of General and Inorganic Chemistry of the Russian Academy of Sciences, Moscow, Russia
[3]Institute for Biological Instrumentation of the Russian Academy of Sciences, Pushchino, Russia

[a]sonyoru162@gmail.com, [b]sergey12-17@yandex.ru, [c]viktoriya.anikina@list.ru,
[d]antonpopovleonid@gmail.com, [e]marina.shevelyova@gmail.com, [f]nellipopovaran@gmail.com

Corresponding author: Nelli R. Popova, nellipopovaran@gmail.com

ABSTRACT Cerium oxide nanoparticles (CeNPs) are among the most promising materials with pH-sensitive redox-activity for biomedical nanotechnologies. CeNPs are known to reduce the toxicity of the chemotherapeutic drug doxorubicin (DOX) for normal cells. Here we have proposed and analyzed a new hybrid cerium/silica containing SiNPs@DOX@CeNPs nanocomposite. We showed that the average size of the nanocomposite is 190 nm and it has a spherical shape. The SiNPs@DOX@CeNPs nanocomposite provides effective synergistic anticancer activity of CeNPs with doxorubicin (DOX), as well as selective toxicity against human osteosarcoma (MNNG/HOS) cells *in vitro*. The SiNPs@DOX@CeNPs nanocomposite may be a good candidate to increase the effectiveness of cancer doxorubicin chemotherapy.

KEYWORDS nanocomposites, silica nanoparticles, cerium oxide nanoparticles, biomedical application, characterization, drug delivery

ACKNOWLEDGEMENTS This research was funded by the Russian Science Foundation, grant number 22-63-00082 and performed using the equipment of the Joint Research Centre for Physical Methods of Research at Kurnakov Institute of General and Inorganic Chemistry of the Russian Academy of Sciences (JRC PMR IGIC RAS).

FOR CITATION Zamyatina E.A., Kottsov S.Yu., Anikina V.A., Popov A.L., Shevelyova M.P., Popova N.R. Cerium oxide@silica core-shell nanocomposite as multimodal platforms for drug release and synergistic anticancer effects. *Nanosystems: Phys. Chem. Math.*, 2023, **14** (5), 560–570.

1. Introduction

Currently, nanomaterials are being widely studied as potential means of increasing the bioavailability of drugs and the effectiveness of therapy for socially significant diseases [1–4]. Cerium oxide nanoparticles (CeNPs) hold a special place among engineered nanomaterials due to the wide range of their enzyme-like activities and bioavailability. They possess superoxide dismutase-, catalase- and peroxidase-like properties, as well as recently discovered phosphatase-, photolyase-, phospholipase-, nuclease-, lipo- and phospholipoperoxidase-like properties [5]. This makes CeNPs a unique multifunctional nanozyme and expands the scope of its future biomedical applications [6–8]. Moreover, it is known that CeNPs increases the bioavailability of a number of biologically active compounds, for example, curcumin [9], and also provides selective redox activity of widely used therapeutic agents for example, doxorubicin (DOX) [10, 11].

DOX has been widely acknowledged as the most commonly used anticancer drug for several decades [12]. However, DOX administration is related to some side effects including the toxicity to multiple organs as well as resistance development towards DOX of cancer cells [13–15]. The use of nanoscale carriers, silica nanoparticles (SiNPs) belong to, is considered as potential solution to increase the performance on tumor cells and reduce the adverse effects on normal cells of DOX due to their ability to access efficaciously into tumor cells [16]. Interestingly, CeNPs with their concomitant administration with DOX managed to mitigate doxorubicin-induced hepatic insult on both histological and biochemical aspects in rats. Recently, an inspiring *in vitro* study [17] has reported that the co-administration of CeNPs with DOX could boost its anti-neoplastic activity in melanoma cells without hampering the viability of normal stromal cells [10]. Moreover, cerium-based nanomaterials were found to enhance the chemosensitization of cancer cells rather than normal cells [11].

Moreover, it has been revealed that the biomimetic enzyme activity of the CeNPs was positively correlated with its surface area-to-volume ratio [18]. It is nanocrystalline cerium oxide of 2 – 10 nm size that most clearly manifests its biological activity, which was shown *in vitro* and *in vivo* [19, 20]. However, due to the ultrasmall size of CeO_2 particles,

short circulation half-time and interparticle agglomeration are anticipated, which compromises the bioavailability and enzyme-like activity of the CeNPs in the targeted site.

SiNPs can be used to accommodate ultrasmall CeNPs to solve this problem. SiNPs have been widely studied as effective systems for the delivery of therapeutic and diagnostic agents to combat various types of diseases, including diabetes, oncological diseases, and diseases accompanied by inflammatory processes [21–25]. It has been shown that, when ingested, SiNPs are rapidly degraded in the excretory organs to orthosilicic acid and excreted in the urine [26–28]. In addition, this approach will also make it possible to combine a model therapeutic agent (DOX) in one nanocomposite. There are several studies showing the possibility of using SiNPs to deliver DOX and CeNPs separately [18, 29]. We found only one paper where the responsive system was designed based on CeNPs coated DOX and photosensitizer hematoporphyrin dual-loaded mesoporous SiNPs for synergetic chemotherapy and photodynamic therapy [30].

Thus, the aim of the present study is to combine CeNPs and DOX in a single nanocomposite using simple SiNPs synthesis technique as a basis in order to analyze their properties and selective toxicity *in vitro*. The results obtained are of special importance for advancing the pharmacotherapeutic applications of CeNPs for the treatment of socially significant diseases and development of synergetic chemotherapy.

2. Materials and methods

2.1. Materials

Tetraethoxysilane (TEOS) (purity $\geq$ 99.0 %) was obtained from Sigma-Aldrich (USA), aqueous ammonia (25 %) was purchased from Dia-M (Russia), ethanol (purity 94 – 96 %, ACS) was obtained from Alfa Aesar (USA), anhydrous copper (II) sulfate (purity $\geq$ 99.0 %) was purchased from Acros Organics (Belgium). CeNPs were obtained from Kurnakov Institute of General and Inorganic Chemistry of the Russian Academy of Sciences. DOX was obtained from Teva Pharmaceutical Industries (Israel).

2.2. SiNPs synthesis

The synthesis procedure was carried out using the Stöber method [31]. Ethanol was preliminarily dried to reduce the amount of H_2O entering the system. To do this, anhydrous copper (II) sulfate was added to 94 – 96 % ethanol, kept for 24 h, and then the resulting ethanol was filtered off. The process of ethyl alcohol drying was carried out for 14 days. Then, 0.2 M ammonia was added to 50 ml of anhydrous ethanol, then the beaker was placed on a magnetic stirrer and the solution was stirred (500 rpm) at room temperature for 10 minutes. Then 0.1 M TEOS was added dropwise, the resulting solution was stirred for 1 hour. Mixture solutions were centrifuged at 6000 rpm for 20 minutes, then washed with anhydrous ethanol and deionized water. The washing cycle was repeated until the required pH was reached. After each step of the synthesis, the pH of the solutions was measured to control the rate of reactions under alkaline conditions (pH $>$ 10). The resulting SiNPs sol in water after completion of all stages was stored at a temperature of 4 °C. Then, other types of SiNPs were synthesized with a change in one of the synthesis parameters in the established range (Table 1), while the remaining characteristics corresponded to the standard protocol presented above.

2.3. CeNPs synthesis

The aqueous sol of CeNPs stabilized by citrate ions was prepared according to the procedure below: 0.24 g of citric acid was dissolved in 25 ml of 0.05 M aqueous solution of cerium (III) nitrate. This solution was rapidly added to 100 ml of 3 M ammonia solution under stirring and kept for 2 h. A stable sol of CeNPs is thus obtained [32].

TABLE 1. SiNPs samples obtained by variations in synthesis characteristics (ammonia, ethanol, TEOS) using the Stöber method

Sample name	Ammonia concentration, M	Ethanol volume, ml	TEOS concentration, M
A	0.2	50	0.1
B	0.5	50	0.1
C	0.6	50	0.1
D	1.2	50	0.1
E	0.2	25	0.1
F	0.2	75	0.1
G	0.2	50	0.04
H	0.2	50	0.2

2.4. SiNPs@DOX@CeNPs synthesis

The following was done for the modification of nanoparticles with DOX: 900 μl of water was added to 100 μl of SiNPs particles. Then DOX was added to SiNPs at concentrations of 0.5, 1, 2.5, 5 mg/ml. The resulting solutions were mixed on a rotary mixer for 24 h in the dark. Then the pH of the solutions was adjusted to 7.8 with 0.1 M Na_2HPO_4. The resulting nanoparticles were collected by centrifugation (9000 rpm, 10 min) and washed with deionized water three times. The amount of loaded DOX was analyzed by spectrophotometry as detailed below in 2.5. Then the ratio of SiNPs and CeNPs was 1:1.43 to modify the nanoparticles. CeNPs were added in concentration 200 mg/ml to SiNPs solution, then the solution was placed in the ultrasonic bath for 1 minute, after which the nanoparticles were left to mix on a rotary mixer for 15 h [33]. The nanoparticles were collected by centrifugation (9000 rpm, 20 min) and washed 3 times with deionized water.

2.5. DOX loading

The amount of loaded DOX was measured by spectrophotometry using a microplate spectrophotometer Multiscan FC (Thermo Fisher, USA) with a detection wavelength of 480 nm. The encapsulation efficiency (EE) was calculated as amount of DOX loaded in SiNPs/amount of drug added $\times$ 100 %; loading capacity (LC) was calculated as amount of DOX in SiNPs/amount of SiNPs $\times$ 100 % [29].

$$EE\ (\%) = \left[\left(\frac{\text{Amount of DOX loaded into SiNP}}{\text{Initial amount of DOX}}\right)\right] \times 100,$$

$$LC\ (\%) = \left[\left(\frac{\text{Initial amount of DOX – amount of DOX supernatant}}{\text{Amount of MSN + amount of DOX}}\right)\right] \times 100.$$

2.6. Nanoparticles size, shape, ζ-potential and EDX analysis

Size of nanoparticles was measured by scanning electron microscopy (SEM) using an NVision 40 microscope (Carl Zeiss, Germany) at an accelerating voltage of 3 kV. The shape of the nanoparticles was analyzed by transmission electron microscopy (TEM) using a JEM-1011 electron microscope (JEOL, Japan). The chemical composition analysis (energy dispersive X-ray analysis, EDX) of the samples was performed using a Carl Zeiss NVision 40 field emission scanning electron microscope equipped with an Oxford Instruments Oxford Instruments INCA (80 mm^2) detector, at an accelerating voltage of 20 kV. The hydrodynamic diameter and ζ-potential of the resulting nanoparticles were measured using dynamic light scattering (DLS) and electrophoretic light scattering (ELS) with a Zetasizer Nano ZS nanoparticle characterization system (Malvern Panalytical, UK). The measurements were carried out at 25 °C. Each measurement represented an average of 15 runs (the number of runs was determined automatically by the instrument). The signals were analyzed using a single-plate multichannel correlator coupled to computer equipped with the Zetasizer Software package for estimating the diameters by the distribution analysis model. All the samples were measured at least 5 times; the average measurement error was about 5 %.

2.7. BET surface area analysis

SiNPs specific surface area (SBET) was determined using a low-temperature nitrogen adsorption device Sorbtometer-M (Katakon, Russia) using the Brunauer–Emmett–Teller (BET) model based on experimental data in P/P_0 range of 0.05 – 0.25. Before the measurements, the samples were outgassed for 1 h at 200 °C under a nitrogen flow.

2.8. FTIR-spectroscopy

The Fourier-transform infrared (FTIR) spectra of the samples were obtained using a Spectrum 65 FT-IR spectrometer (Perkin Elmer, USA) with a Quest ATR attenuated total reflection (ATR) accessory (Specac, UK) in the wavenumber range of 400 – 4000 cm^{-1}.

2.9. Raman spectroscopy

Raman spectra were obtained using a Confotec NR500 Raman microscope (Sol Instruments, Belarus) at 633 nm excitation laser wavelength operating at $\sim$3 mW power using $\times$40 magnification lens (NA = 0.75).

2.10. Cell culture

Human Mesenchymal Stem cells (hMSc) were isolated from the tooth pulp of a healthy donor, according to orthodontic prescription and with the informed consent of the patient. All procedures were carried out in accordance with the approved clinical rules for biomaterial sampling. Human Bone Osteosarcoma (MNNG/HOS) cell culture was obtained from the Cryobank of the Institute of Cell Biophysics of the Russian Academy of Science (Russia). hMSc and MNNG/HOS were cultured in Dulbecco's Modified Eagle's Medium (DMEM)/F12 (1:1) with the addition of 10 % fetal bovine serum and 100 U/ml penicillin/streptomycin under 5 % CO_2 at 37 °C.

2.11. MTT assay

The determination of mitochondrial and cytoplasmic dehydrogenases activity in living cells was carried out using a MTT assay based on the reduction of the colorless tetrazolium salt (3-[4.5-dimethylthiazol-2-yl]-2.5-diphenyltetrazolium bromide, MTT, Sigma-Aldrich, USA). Briefly, SiNPs, SiNPs@CeNPs, SiNPs@DOX@CeNPs, DOX and CeNP were added to cells growing in 96-well plates (for 24, 48 and 72 h at 37 °C in humid air (98 %) containing 5 % CO_2). 3 h prior to the end of the exposure period, the supernatant was removed, and MTT solution in phosphate-buffered saline (0.5 mg/mL, 100 μL/well) was added to the cells for 10 min. Upon the completion of the exposure period, the supernatant was removed, and a lysis solution containing 0.1 % sodium dodecyl sulfate (Sigma-Aldrich, USA) solution in dimethyl sulfoxide was added. Plates were shaken for 10 min, placed on a microplate spectrophotometer Multiskan FC (Thermo Fisher, USA), and the absorbance was read colorimetrically at 570 nm. Each experiment was repeated three times, with five replications.

2.12. Live/dead assay

Cell viability after exposure to nanoparticles was assessed using a Carl Zeiss Axiovert 200 microscope. Cells were seeded into 96-well plates and stained with Hoechst 33342 fluorescent dye (absorption – 350 nm, emission – 461 nm) and a propidium iodide dye (absorption – 493 nm, emission – 636 nm). The dyes were added to the DMEM/F12 without serum (1 μg/ml) and the plate was placed in a CO_2 incubator for 15 min. Microphotographs were taken after washing the cells with a phosphate-buffered saline. For each cell group, four fields in each well were examined. The number of cells (total cells/dead cells) was calculated using the ImageJ software.

3. Results and discussion

3.1. Synthesis, properties and characterization of nanoparticles

3.1.1. Synthesis, properties and morphology of SiNPs. To obtain SiNPs, the Stöber method is widely used [31], being one of the most widespread and easy-to-control methods for obtaining nanoparticles of controlled size, shape, and morphology [34]. For the biomedical applications the preferred nanoparticles size is to be in the range of 10 – 150 nm. This is due to the fact that nanoparticles smaller than 10 nm are rapidly excreted by the renal system. On the other hand, too large nanoparticles (more than 200 nm) do not pass through endothelial pores. Optimizations of the synthesis conditions are required to achieve the optimal SiNPs size. The influence of the concentrations of TEOS/ethanol/ammonia on the size and morphology of the synthesized SiNPs was studied (Table 1). The particle size and other structural characteristics the concentrations of the precursors of each sample are shown in Table 2.

TABLE 2. Main characteristics of SiNPs

Sample name	Particle diameter (SEM), nm	Hydrodynamic diameter in deionized water, nm	ζ-potential in deionized water, mV	PDI
A	70 ± 6	140 ± 12	-53.6 ± 1.8	0.14 ± 0.02
B	77 ± 13	285 ± 23	-54.5 ± 2.5	0.19 ± 0.01
C	110 ± 17	253 ± 21	-30.1 ± 1.4	0.15 ± 0.01
D	682 ± 28	755 ± 17	-10.2 ± 1.5	0.73 ± 0.02
E	77 ± 9	126 ± 16	-53.5 ± 0.9	0.16 ± 0.01
F	282 ± 10	403 ± 26	-45.8 ± 1.7	0.51 ± 0.02
G	94 ± 11	104 ± 15	-46.2 ± 1.4	0.28 ± 0.01
H	342 ± 15	363 ± 19	-59.4 ± 2.3	0.24 ± 0.01

The size of the nanoparticles was investigated using DLS and SEM (Table 2, Fig. 1) methods. TEOS acts as a silica precursor for the synthesis of SiNPs, and its concentration affects the rate of seed growth and nucleation [32]. An increase in TEOS concentration raises the number of hydrolyzed silicic acid monomers and ultimately the size of SiNPs. For the 0.1 M TEOS, the nanoparticles have optimal size for biological applications (hydrodynamic diameter is 140 ± 12 nm (ζ-potential of -53.6 ± 1.8 mV) with low PDI values of 0.14 ± 0.02). The PDI values confirm high homogeneity of the samples. Ammonia used during Stöber synthesis acts as a catalyst for the hydrolysis of TEOS (silica precursor), i.e., partially to fully hydrolyzed silanol monomers are produced with increasing ammonia concentration. It enhances the degree of polymerization/condensation and hence leads to the larger SiNPs. Less hydrolyzed monomers are produced at lower ammonia concentration resulting in the small-sized SiNPs. With an increase of ammonia concentration from 0.2 to 1.2 M, the particle size increased from 70 to 680 nm. It is known that there is a correlation between the ammonia

concentration and the size of silica spheres, which is associated with the processes of increasing polymerization [31, 35]. Smaller size of spherical SiNPs was obtained using a lower concentration of ethanol. This may indicate that the solvent interacts with silanol groups (Si–O–H) in the formation of SiNPs. The particle size increases with the length of the alcohol chain [36].

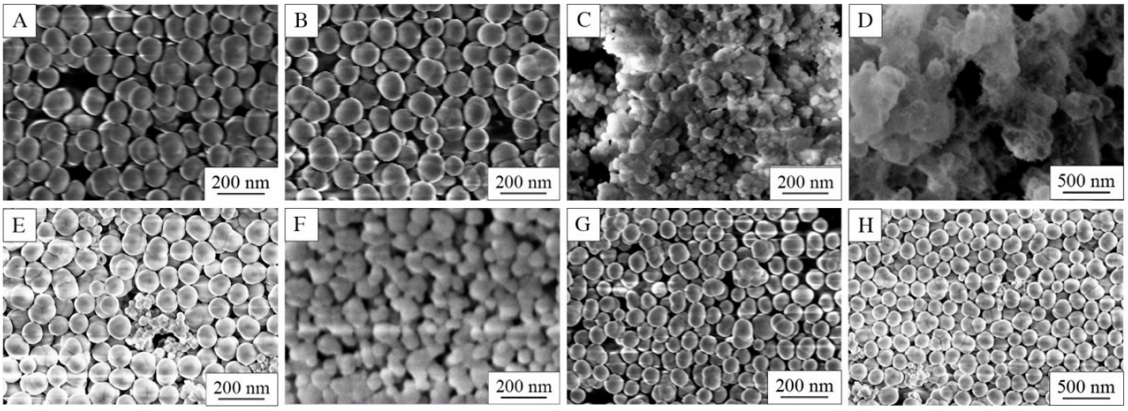

FIG. 1. SEM images of SiNPs obtained by varying concentrations of ammonia: 0.2 M (A); 0.5 M (B); 0.6 M (C) and 1.2 M (D); by varying the volume of ethanol: 25 ml (E) and 75 ml (F); by varying the concentration of TEOS 0.04 M (G), 0.2 M (H)

The morphology of SiNPs was observed using SEM images (Fig. 1). SiNPs showed uniform particle distribution with a diameter of 70 to 670 nm. All synthesized SiNPs have spherical shape. Spherical nanoparticles with hydrodynamic diameter of 140 ± 12 nm were chosen for the further modification in this study.

SiNPs specific surface area was measured to be $S_{BET} = 19$ m^2/g (Sample A, Tables 1, 2). That value corresponds to smooth spherical SiNPs ($\rho = 2.1$ g/cm^3) of about 150 nm in diameter d [nm] $= \dfrac{6 \cdot 10^3}{p \cdot S_{BET}}$, which is significantly higher than the particle size estimated from SEM (70 ± 6 nm). Thus, the obtained surface area value is probably underestimated due to BET method experimental error [37] and SiNPs aggregation during the sample degassing stage.

3.1.2. SiNPs@DOX, SiNPs@CeNPs, SiNPs@DOX and SiNPs@DOX@CeNPs synthesis and properties. SiNPs were synthesized by the method described above. At the next stage, DOX was conjugated to the SiNPs surface. In order to confirm the adsorption of DOX on SiNPs surface and the absence of the chemical interaction between them, an FTIR and Raman spectroscopy study was carried out (Fig. 2).

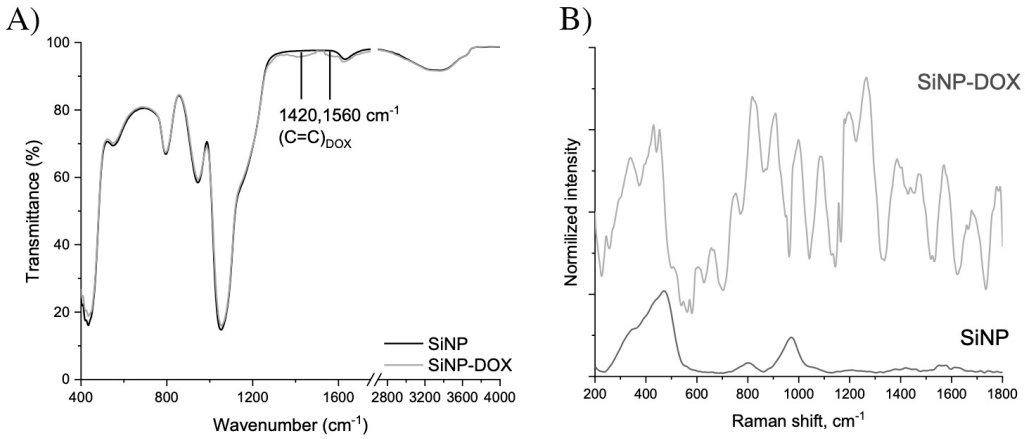

FIG. 2. (a) FTIR and (b) Raman spectra of SiNPs loaded with DOX

FTIR spectrum of SiNPs is typical for sol-gel silica nanoparticles with, all major silica bands vibrations present: bending O–Si–O (434 cm^{-1}), breathing (Si–O)$_3$ cycle vibrations (548 cm^{-1}) and Si–O–Si stretching vibrations (796, 1054 and 1200 (shoulder) cm^{-1}) [38]. The peak at 946 cm^{-1} is attributed to Si–OH stretching vibrations at nanoparticles surface; the presence of OH-groups is also confirmed by the negative δ-potential of SiNPs (Table 2). The bands of bending (1630 cm^{-1}) and stretching ($\sim$ 3300 cm^{-1}) vibrations of residual water in SiNPs are also present [39]. The

FTIR spectrum of the nanoparticles barely changed after the DOX loading. The only new vibration bands appeared at 1420 and 1560 cm^{-1} which can be attributed to C=C bond vibrations in the aromatic structure of DOX [38–40].

To reliably confirm DOX loading at SiNPs, Raman spectroscopy was used due to its better sensitivity to nonpolar, but polarizable moieties [41], such as aromatic system of DOX molecule. Spectrum of bare SiNPs was also typical for SiNPs: bonds at 354 (O–Si–O deformation), 469 (HO–SiO_3 breathing mode), 801 (Si–O–Si stretching) and 972 cm^{-1} (Si–OH asymmetric stretching) were observed [38, 42]. After DOX incorporation in SiNPs many new vibration bands were registered in Raman spectrum indicating the successful DOX adsorption, with the main characteristic DOX bands at 454 and 1082 cm^{-1} (deformation C–O vibrations), 996 cm^{-1} (C–C ring breathing vibration), 1201 and 1265 cm^{-1} (combinational modes of ring breathing vibrations and OH band deformation), and 1571 cm^{-1} (non-aromatic ring stretching) [38,42–44]. No noticeable band wavelength shift was registered for SiNPs@DOX composite compared to pure DOX indicating the lack of chemical interaction between silica and DOX.

DOX loading was studied using different concentrations of DOX, the evaluation of the SiNPs modification efficiency was carried out by calculating the EE and LC parameters. EE and LC values of DOX in SiNPs are shown in Table 3. With an increase in the concentration of loaded DOX from 0.5 to 5 mg/ml, the EE of the drug increased from 90.69 to 98.99 %. Also, the drug loading capacity increased from 75.57 to 97.04 %. Thus, in the further study, the DOX concentration of 5 mg/ml was selected for the fabrication of SiNPs@DOX. SiNPs are effectively loaded with DOX mainly due to the physical adsorption.

TABLE 3. Encapsulation efficiency (EE) and loading capacity (LC) of DOX in SiNPs

Amount of loaded DOX, mg/ml	EE, %	LC, %
0.5	90.69	75.57
1	95.34	86.68
2.5	98.13	94.36
5	98.99	97.04

At the second stage, SiNPs@DOX were conjugated with CeNPs. In this study, we used a simple procedure for the synthesis of stable aqueous cerium oxide sols and studied the effect of the concentration and molar ratio of the initial reagents on the size of CeNPs [32]. The average size of CeNPs was about 5 nm by TEM (Fig. 3A), while an average hydrodynamic diameter of CeNPs was 16 ± 4 nm (Table 4). The average hydrodynamic diameter of SiNPs without DOX and CeNPs was 140 ± 12 nm. The size of the SiNPs modified with CeNPs was 123 ± 3 nm. Adsorption of DOX to the SiNPs led to increasing nanoparticles' hydrodynamic diameter to 150 ± 17 nm (ζ-potential of -23.7 ± 2.0 mV). Adsorption of CeNPs on the SiNPs@DOX led to increasing the nanocomposite hydrodynamic size to 198 ± 13 nm. This increase indicates that CeNPs were adsorbed on the surface. Measurements of the SiNPs@DOX@CeNPs diameter were also carried out using the SEM method (Fig. 4), which confirmed an average size of about 190 nm. SiNPs@DOX@CeNPs nanocomposite has a spherical shape which was confirmed by TEM (Fig. 3B).

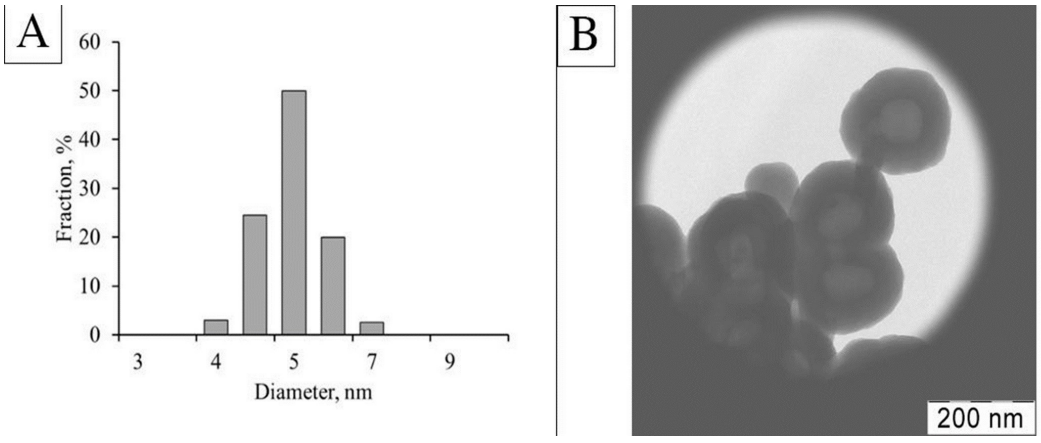

FIG. 3. Size distribution of CeNPs (A), TEM high magnification image of SiNPs modified by DOX and CeNPs (SiNPs@DOX@CeNPs) (B)

The chemical composition of SiNPs@DOX@CeNPs nanoparticles was confirmed with EDX analysis (Fig. 5). As expected, only Si, Ce, O and C elements were found. The Si:Ce (SiO_2:CeO_2) ratio in the sample was 9:1, and the difference in SiO_2:CeO_2 ratios measured in ten different locations did not exceed 1 %.

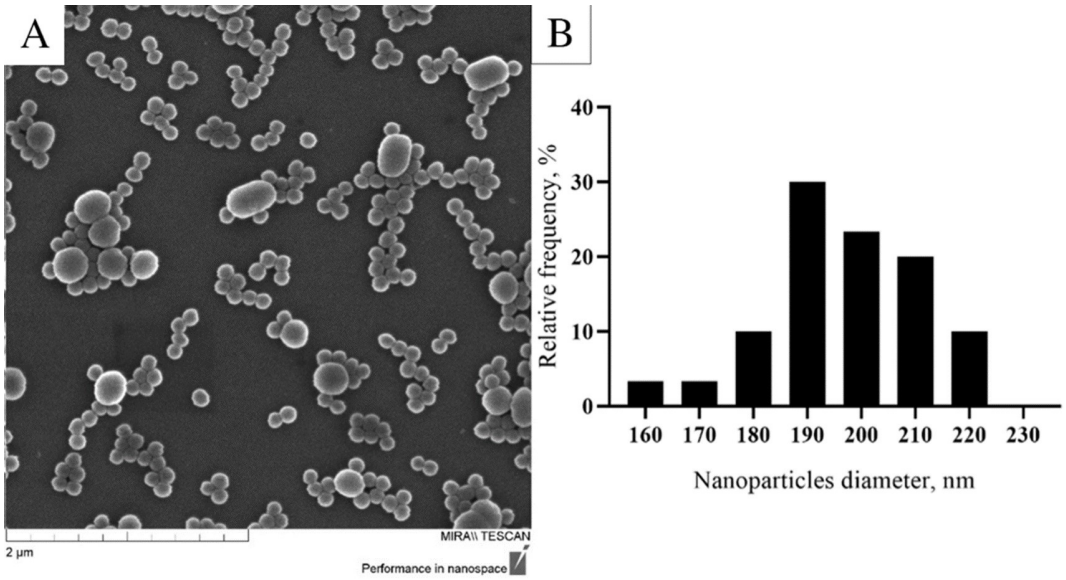

FIG. 4. SEM image of SiNPs modified by DOX and CeNPs (SiNPs@DOX@CeNPs) (A); size distribution of SiNPs@DOX@CeNPs (B)

TABLE 4. Physical characteristics of the core-shell nanocomposite and its individual components

Samples	Hydrodynamic diameter, nm	ζ-potential, mV
SiNPs	140 ± 12	-53.6 ± 1.8
CeNPs	16 ± 4	-41.7 ± 1.2
SiNPs@CeNPs	123 ± 3	-31.2 ± 2.1
SiNPs@DOX	150 ± 17	-19.4 ± 2.4
SiNPs@DOX@CeNPs	198 ± 13	-23.7 ± 2.0

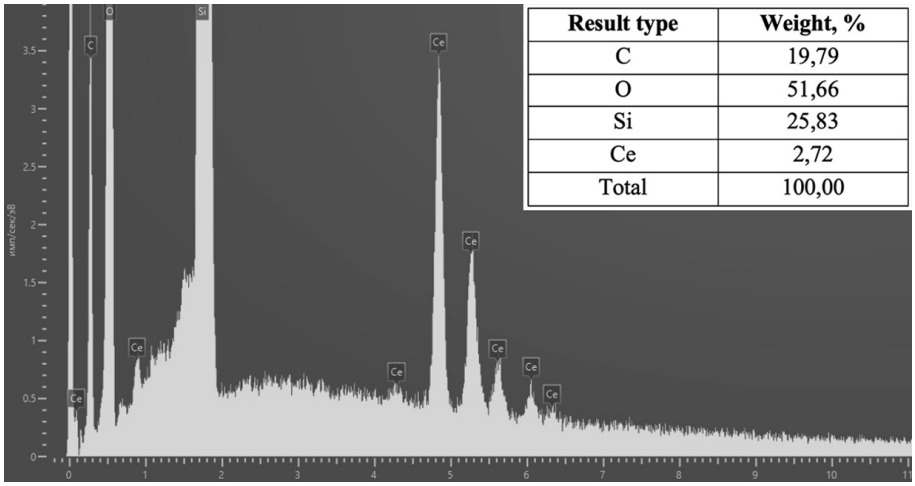

Result type	Weight, %
C	19,79
O	51,66
Si	25,83
Ce	2,72
Total	100,00

FIG. 5. EDX spectrum of SINPs@DOX@CeNPs

3.2. Cytotoxicity study of SiNPs@DOX@CeNPs

The cytotoxicity of the SiNPs, free DOX, CeNPs, SiNPs@CeNPs, SiNPs@DOX@CeNPs was assessed using MTT method and Live/Dead assay (cell viability analysis by fluorescent dye staining). Human mesenchymal stem cells (hMSc) and human bone osteosarcoma cells (MNNG/HOS) were separately incubated with SiNPs, free DOX, CeNPs, SiNPs@CeNPs, SiNPs@DOX@CeNPs (70 μM) for 24, 48 and 72 h. The concentration of 70 μM was chosen as the optimal for detecting biological effects, while being non-toxic. The cell cultures were chosen because DOX [45–47] is often used for osteosarcoma chemotherapy, and so it is of primary importance to establish how new nanocomposite could affect cancer cells. Mesenchymal stem cells were used to study the effect of the nanocomposite on normal cells. As it is shown in Fig. 6 the dehydrogenase activity of hMSc was not decreased upon incubation with all tested the types of nanoparticles for three days. On the contrary, DOX provided a decrease in activity up to 50 % by 72 h of incubation. The results of cell viability analysis by fluorescent staining showed that the nanoparticles upon incubation during 24, 48 and 72 h with hMSc did not have a cytotoxic effect in the concentration (Fig. 7). IC_{20} and IC_{50} for SiNPs, CeNPs, SiNPs@CeNPs, SiNPs@DOX@CeNPs were not detected. The ratio of dead cells to total cells increased by 30 – 50 % compared to the intact control in experiments with hMSc incubation with DOX.

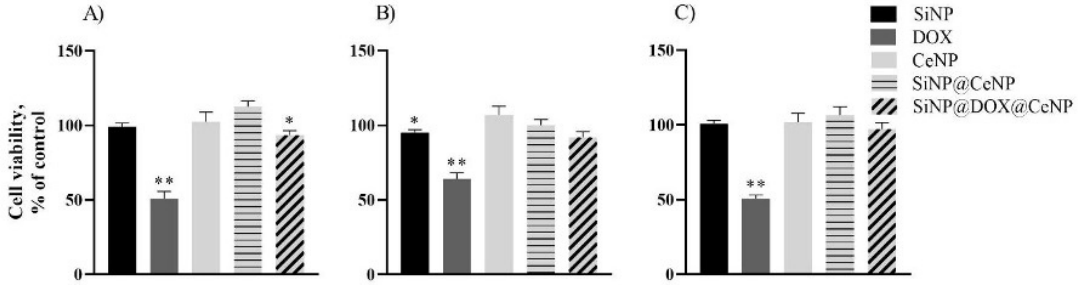

FIG. 6. MTT assay results obtained on human mesenchymal stem cells (hMSc) *in vitro*. The test was carried out after 24 (A), 48 (B), and 72 (C) h. Results are represented as a mean $\pm$ SD. The values of the metabolic activity of cells are shown as a percentage of the control. Statistical significance was assumed for P-values < 0.05: ($^*P < 0.05$, $^{**}P < 0.01$)

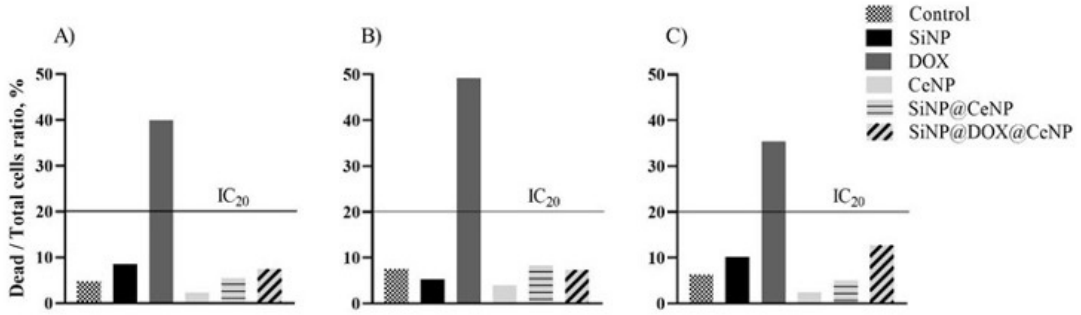

FIG. 7. Live/dead test results obtained on human mesenchymal stem cells (hMSc) *in vitro*. The test was carried out after 24 (A), 48 (B), and 72 (C) h of cell incubation with tested samples at a concentration of 70 μM. The values are indicated as a percentage of the number of dead cells to their total number

24 h after incubation of MNNG/HOS with free DOX, the dehydrogenase activity of cells (Fig. 8) was comparable to control values, and no decrease in dehydrogenase activity was observed in the case of incubation with SiNPs@DOX@CeNPs. Therefore, during incubation for 48 h with free DOX, no significant differences were observed with the control. During the incubation of MNNG/HOS with SiNPs@DOX@CeNPs, dehydrogenase activity decreased by 45 % compared to the intact control. When the MNNG/HOS is incubated for 72 h with free DOX, 25 % decrease in the dehydrogenase activity of the cells is observed compared to the control. In the case of MNNG/HOS incubation with SiNPs@DOX@CeNPs, the dehydrogenase activity of cells decreased by 65 % compared to the control. Thus, the MNNG/HOS cell culture, despite the initial decrease in dehydrogenase activity, showed resistance to free doxorubicin over time. On the contrary, DOX incorporated SiNPs@CeNPs had an inhibitory effect on the viability of MNNG/HOS after three days of incubation with SiNPs@DOX@CeNPs. Live/dead test results show (Fig. 9) an increase in the number of dead cells up to almost 80 %

with SiNPs@DOX@CeNPs incubation. The effect shown on cell cultures may be due to the fact that CeNPs possess self-regenerative, redox-responsive dual-catalytic activities, thus attracting interest as an innovative means to treating cancer [48–50]. Depending on surface characteristics and environment, CeNPs exerts either anti- or pro-oxidative effects which regulate reactive oxygen species (ROS) levels in biological systems. CeNPs mimics ROS-related enzymes that protect normal cells at physiological pH range from oxidative stress and induce ROS production in the slightly acidic tumor microenvironment to trigger cancer cell death [51, 52].

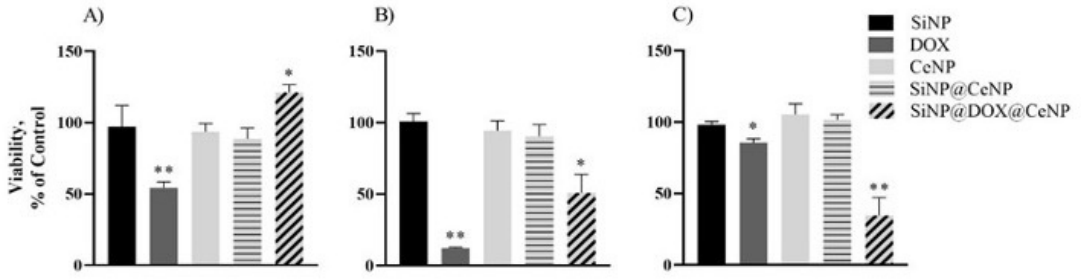

FIG. 8. MTT assay results obtained on human bone osteosarcoma cells (MNNG/HOS) *in vitro*. The test was carried out after 24 (A), 48 (B), and 72 (C) h of cell incubation with tested samples at a concentration of 70 μM. Results are shown as a mean $\pm$ SD. The values of the metabolic activity of cells are indicated as a percentage of the control. Statistical significance was assumed for P-values < 0.05: ($^*P < 0.05$, $^{**}P < 0.01$

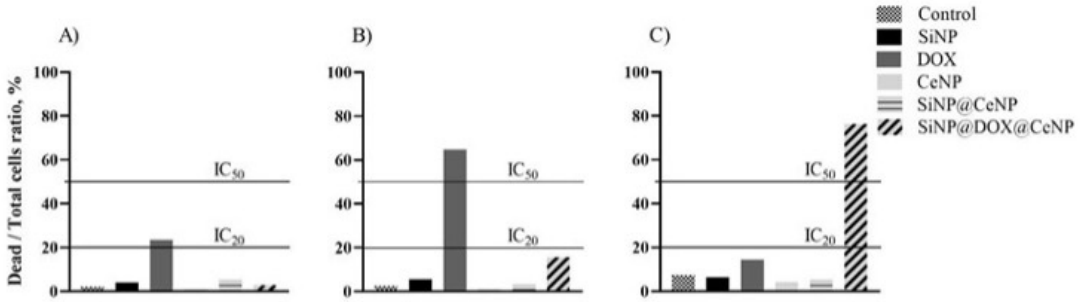

FIG. 9. Live/dead test results obtained on human bone osteosarcoma cells (MNNG/HOS) *in vitro*. The test was carried out after 24 (A), 48 (B), and 72 (C) h of cell incubation with tested samples at a concentration of 70 μM. The values are shown as a percentage of the number of dead cells to their total number

The results obtained, indicated that SiNPs@DOX@CeNPs provided high cytotoxicity to cancer cells while having protective effect on normal cells.

4. Conclusions

Herein, a new hybrid nanocomposite SiNPs@DOX@CeNPs based on silica nanoparticles (SiNPs), doxorubicin (DOX) and cerium oxide nanoparticles (CeNPs) were proposed as multimodal platform having selective cytotoxicity to cancer cells. The synthesized nanocomposite was characterized by SEM, TEM, FTIR, DLS and Raman spectroscopy. The average size of the nanoparticles is 190 nm. The proposed drug loading method provides a high doxorubicin capacity (over 90 %). SiNPs@DOX@CeNPs demonstrated low toxicity to the human mesenchymal stem cell line, while exhibited high toxicity to osteosarcoma cells reducing their viability by up to 30 % compared to untreated control. CeNPs enhance the cytotoxic effect of doxorubicin when introduced in the nanocomposite. The SiNPs@DOX@CeNPs has a great potential for effective drug delivery aimed at increasing the efficiency of cancer treatment.

References

[1] Sozarukova M.M., Ivanov V.K., Shestakova M.A., et.al. Quantification of free radical scavenging properties and SOD-like activity of cerium dioxide nanoparticles in biochemical models. *Russ. J. Inorg. Chem.*, 2020, **65**, P. 597–605.

[2] Kozlova T.O., Popov A.L., Romanov M.V., et al. Ceric phosphates and nanocrystalline ceria: selective toxicity to melanoma cells. *Nanosystems: Phys. Chem. Math.*, 2023, **14**, P. 223–230.

[3] Zhu W., Wei Z., Han C., Weng X. Nanomaterials as Promising Theranostic Tools in Nanomedicine and Their Applications in Clinical Disease Diagnosis and Treatment. *Nanomaterials*, 2021, **11**, 3346.

[4] Yusuf A., Almotairy A.R.Z., Henidi H., Alshehri O.Y., Aldughaim M.S. Nanoparticles as Drug Delivery Systems: A Review of the Implication of Nanoparticles' Physicochemical Properties on Responses in Biological Systems. *Polymers*, 2023, **15**, 1596.

[5] Sozarukova M.M., Proskurnina E.V., Popov A.L., Kalinkin A.L., Ivanov V.K. New Facets of Nanozyme Activity of Ceria: Lipo- and Phospholipoperoxidase-like Behaviour of CeO_2 Nanoparticles. *RSC Adv.*, 2021, **11**, P. 35351–35360.

[6] Rajeshkumar S., Naik P. Synthesis and Biomedical Applications of Cerium Oxide Nanoparticles – A Review. *Biotechnol. Rep. Amst. Neth.*, 2018, **17**, P. 1–5.

[7] Dhall A., Self W. Cerium Oxide Nanoparticles: A Brief Review of Their Synthesis Methods and Biomedical Applications. *Antioxid. Basel Switz.*, 2018, **7**, 97.

[8] Shcherbakov A.B., Reukov V.V., Yakimansky A.V., Krasnopeeva E.L., Ivanova O.S., Popov, A.L., Ivanov V.K. CeO_2 Nanoparticle-Containing Polymers for Biomedical Applications: A Review. *Polymers*, 2021, **13**, 924.

[9] Shirokikh A.D., Anikina V.A., Zamyatina E.A., Mishchenko E.V., Koroleva M.Y., Ivanov V.K., Popova N.R. Bioavailability of Nanoemulsions Modified with Curcumin and Cerium Dioxide Nanoparticles. *Nanosyst. Phys. Chem. Math.*, 2023, **14**, P. 89–97.

[10] Ibrahim H.G., Attia N., Hashem F.E.Z.A., El Heneidy M.A.R. Cerium Oxide Nanoparticles: In Pursuit of Liver Protection against Doxorubicin-Induced Injury in Rats. *Biomed. Pharmacother. Biomedecine Pharmacother.*, 2018, **103**, P. 773–781.

[11] Wu G., Zhang Z., Chen X., Yu Q., Ma X., Liu L. Chemosensitization Effect of Cerium Oxide Nanosheets by Suppressing Drug Detoxification and Efflux. *Ecotoxicol. Environ. Saf.*, 2019, **167**, P. 301–308.

[12] Bahrami Z., Badiei A., Atyabi F. Surface Functionalization of SBA-15 Nanorods for Anticancer Drug Delivery. *Chem. Eng. Res. Des.*, 2014, **92**, P. 1296–1303.

[13] Yu F., Tang X., Pei M. Facile Synthesis of PDMAEMA-Coated Hollow Mesoporous Silica Nanoparticles and Their PH-Responsive Controlled Release. *Microporous Mesoporous Mater.*, 2013, **173**, P. 64–69.

[14] Rehman F., Ahmed K., Airoldi C., Gaisford S., Buanz A., Rahim A., Muhammad N., Volpe P.L.O. Amine Bridges Grafted Mesoporous Silica, as a Prolonged/Controlled Drug Release System for the Enhanced Therapeutic Effect of Short Life Drugs. *Mater. Sci. Eng. C*, 2017, **72**, P. 34–41.

[15] Lee S., Kwon J.A., Park K.H., Jin C.M., Joo J.B., Choi I. Controlled Drug Release with Surface-Capped Mesoporous Silica Nanoparticles and Its Label-Free in Situ Raman Monitoring. *Eur. J. Pharm. Biopharm.*, 2018, **131**, P. 232–239.

[16] Nguyen T.N.T., Le N.T.T., Nguyen N.H., Ly B.T.K., Nguyen T.D., Nguyen D.H. Aminated Hollow Mesoporous Silica Nanoparticles as an Enhanced Loading and Sustained Releasing Carrier for Doxorubicin Delivery. *Microporous Mesoporous Mater.*, 2020, **309**, 110543.

[17] Yu J., Wang C., Kong Q., Wu X., Lu J.-J., Chen X. Recent Progress in Doxorubicin-Induced Cardiotoxicity and Protective Potential of Natural Products. *Phytomedicine Int. J. Phytother. Phytopharm.*, 2018, **40**, P. 125–139.

[18] Liu H., Wang J., Wang M., Wang Y., Shi S., Hu X., Zhang Q., Fan D., Xu P. Biomimetic Nanomedicine Coupled with Neoadjuvant Chemotherapy to Suppress Breast Cancer Metastasis via Tumor Microenvironment Remodeling. *Adv. Funct. Mater.*, 2021, **31**, 2100262.

[19] Popov A.L., Popova N.R., Selezneva I.I., Akkizov A.Y., Ivanov V.K. Cerium Oxide Nanoparticles Stimulate Proliferation of Primary Mouse Embryonic Fibroblasts in Vitro. *Mater. Sci. Eng. C Mater. Biol. Appl.*, 2016, **68**, P. 406–413.

[20] Popov A.L., Shcherbakov A.B., Zholobak N.M., Baranchikov A.E., Ivanov V.K. Cerium Dioxide Nanoparticles as Third-Generation Enzymes (Nanozymes). *Nanosyst.: Phys. Chem. Math.*, 2017, P. 760–781.

[21] Fitzmaurice S.D., Sivamani R.K., Isseroff R.R. Antioxidant Therapies for Wound Healing: A Clinical Guide to Currently Commercially Available Products. *Skin Pharmacol. Physiol.*, 2011, **24**, P. 113–126.

[22] Ahsan H., Hadi S.M. Strand Scission in DNA Induced by Curcumin in the Presence of Cu (II). *Cancer Lett.*, 1998, **124**, P. 23–30.

[23] Thomas L., Zakir F., Mirza M.A., Anwer M.K., Ahmad F.J., Iqbal Z. Development of Curcumin Loaded Chitosan Polymer Based Nanoemulsion Gel: In Vitro, Ex Vivo Evaluation and in Vivo Wound Healing Studies. *Int. J. Biol. Macromol.*, 2017, **101**, P. 569–579.

[24] Ahmad N., Ahmad R., Al-Qudaihi A., Alaseel S.E., Fita I.Z., Khalid M.S., Pottoo F.H. Preparation of a Novel Curcumin Nanoemulsion by Ultrasonication and Its Comparative Effects in Wound Healing and the Treatment of Inflammation. *RSC Adv.*, 2019, P. 20192–20206.

[25] Legonkova O.A., Korotaeva A.I., Terekhova R.P., Asanova L.Yu., Shcherbakov A.B., Zholobak N.M., Baranchikov A.E., Krasnova E.V., Shekunova T.O., Ivanov V.K. Method for producing a biologically active composite based on nanocrystalline cerium dioxide and curcumin. Patent RU 2665378 C1, filed October 3, 2017, issued August 29 2018.

[26] Xue Y., Luan Q., Yang D., Yao X., Zhou K. Direct Evidence for Hydroxyl Radical Scavenging Activity of Cerium Oxide Nanoparticles. *J. Phys. Chem. C*, 2011, **115**, P. 4433–4438.

[27] Plakhova T.V., Romanchuk A.Y., Butorin S.M., Konyukhova A.D., Egorov A.V., Shiryaev A.A., Baranchikov A.E., Dorovatovskii P.V., Huthwelker T., Gerber E., et al. Towards the Surface Hydroxyl Species in CeO_2 Nanoparticles. *Nanoscale*, 2019, **11**, P. 18142–18149.

[28] Popova N.R., Shekunova T.O., Popov A.L., Selezneva I.I., Ivanov V.K. Cerium Oxide Nanoparticles Provide Radioprotective Effects upon X-Ray Irradiation by Modulation of Gene Expression. *Nanosystems: Phys. Chem. Math.*, 2019, **10**, P. 564–572.

[29] Kim M.-K., Ki D.-H., Na Y.-G., Lee H.-S., Baek J.-S., Lee J.-Y., Lee H.-K., Cho C.-W. Optimization of Mesoporous Silica Nanoparticles through Statistical Design of Experiment and the Application for the Anticancer Drug. *Pharmaceutics*, 2021, **13**, 184.

[30] Wen J., Yang K., Xu Y., Li H., Liu F., Sun S. Construction of A Triple-Stimuli-Responsive System Based on Cerium Oxide Coated Mesoporous Silica Nanoparticles. *Sci. Rep.*, 2016, **6**, 38931.

[31] Ghimire P.P., Jaroniec M. Renaissance of Stöber Method for Synthesis of Colloidal Particles: New Developments and Opportunities. *J. Colloid Interface Sci.*, 2021, **584**, P. 838–865.

[32] Ivanova O.S., Shekunova T.O., Ivanov V.K., Shcherbakov A.B., Popov A.L., Davydova G.A., Selezneva I.I., Kopitsa G.P., Tret'yakov Yu.D. One-Stage Synthesis of Ceria Colloid Solutions for Biomedical Use. *Dokl. Chem.*, 2011, **437**, P. 103–106.

[33] Shcherbakov A.B., Ivanov V.K. *Practical Manual on Nanomaterials and Nanotechnologies*, Second edition. 2022, 382 p.

[34] Chang H., Kim J., Rho W.-Y., Pham X.-H., Lee J.H., Lee S.H., Jeong D.H., Jun B.-H. Silica Nanoparticles. *Adv. Exp. Med. Biol.*, 2021, **1309**, P. 41–65.

[35] Zeng D., Zhang H., Wang B., Sang K., Yang J. Effect of Ammonia Concentration on Silica Spheres Morphology and Solution Hydroxyl Concentration in Stober Process. *J. Nanosci. Nanotechnol.*, 2015, **15**, P. 7407–7411.

[36] Zainal N.A., Shukor S.R.A., Razak K.A. Study on the effect of synthesis parameters of silica nanoparticles entrapped with rifampicin. *Chem. Eng.*, 2013, **32** (7), P. 432–434.
[37] Thommes M., Kaneko K., Neimark A.V., Olivier J.P., Rodriguez-Reinoso F., Rouquerol J., Sing K.S.W. Physisorption of Gases, with Special Reference to the Evaluation of Surface Area and Pore Size Distribution (IUPAC Technical Report). *Pure Appl. Chem.*, 2015, **87**, P. 1051–1069.
[38] Capozzi C.A., Pye L.D., Condrate R.A. Vibrational Spectral/Structural Changes from the Hydrolysis/Polycondensation of Methyl-Modified Silicates. I. Comparisons for Single Monomer Condensates. *Mater. Lett.*, 1992, **15**, P. 130–136.
[39] Socrates G. *Infrared and Raman Characteristic Group Frequencies: Tables and Charts*, Wiley, 2004.
[40] Bansal R., Singh R., Kaur K. Quantitative Analysis of Doxorubicin Hydrochloride and Arterolane Maleate by Mid IR Spectroscopy Using Transmission and Reflectance Modes. *BMC Chem.*, 2021, **15**, 27.
[41] Smith E., Dent G. *Modern Raman Spectroscopy: A Practical Approach*, John Wiley and Sons, 2005.
[42] Yuan P., He H.P., Wu D.Q., Wang D.Q., Chen L.J. Characterization of Diatomaceous Silica by Raman Spectroscopy. *Spectrochim. Acta. A. Mol. Biomol. Spectrosc.*, 2004, **60**, P. 2941–2945.
[43] Zhang R., Zhu J., Sun D., Li J., Yao L., Meng S., Li Y., Dang Y., Wang K. The Mechanism of Dynamic Interaction between Doxorubicin and Calf Thymus DNA at the Single-Molecule Level Based on Confocal Raman Spectroscopy. *Micromachines*, 2022, **13**, 940.
[44] Gautier J., Munnier E., Douziech-Eyrolles L., et al. SERS spectroscopic approach to study doxorubicin complexes with Fe^{2+} ions and drug release from SPION-based nanocarriers. *Analyst*, 2013, **24**, P. 7354–7361.
[45] Zheng Y., Wang G., Chen R., Hua Y., Cai Z. Mesenchymal stem cells in the osteosarcoma microenvironment: their biological properties, influence on tumor growth, and therapeutic implications. *Stem Cell Research & Therapy*, 2018, **9**, 22.
[46] Wei H., Chen J., Wang S., Fu F., Zhu X., Wu C., Liu Z., Zhong G., Lin J. A Nanodrug Consisting Of Doxorubicin And Exosome Derived From Mesenchymal Stem Cells For Osteosarcoma Treatment In Vitro. *Int. J. Nanomedicine*, 2019, **14**, P. 8603–8610.
[47] Smrke A., Anderson P.M., Gulia A., Gennatas S., Huang P.M., Jones R.L. Future Directions in the Treatment of Osteosarcoma. *Cells*, 2021, **10** (1), 172.
[48] Niu J., Wang K., Kolattukudy P.E. Cerium Oxide Nanoparticles Inhibits Oxidative Stress and Nuclear Factor-KB Activation in H9c2 Cardiomyocytes Exposed to Cigarette Smoke Extract. *J. Pharmacol. Exp. Ther.*, 2011, **338**, P. 53–61.
[49] Ramachandran M., Subadevi R., Sivakumar M. Role of PH on Synthesis and Characterization of Cerium Oxide (CeO_2) Nano Particles by Modified Co-Precipitation Method. *Vacuum*, 2019, **161**, P. 220–224.
[50] Seminko V., Maksimchuk P., Grygorova G., Okrushko E., Avrunin O., Semenets V., Malyukin Y. Mechanism and Dynamics of Fast Redox Cycling in Cerium Oxide Nanoparticles at High Oxidant Concentration. *J. Phys. Chem. C*, 2021, **125**, P. 4743–4749.
[51] Shi X., Tian Y., Zhai S., Liu Y., Chu S., Xiong Z. The Progress of Research on the Application of Redox Nanomaterials in Disease Therapy. *Front. Chem.*, 2023, **11**.
[52] Popov A.L., Kolmanovich D.D., Popova N.R., Sorokina S.S., Ivanova O.S., Chukavin N.N., Shcherbakov A.B., Kozlova T.O., Kalashnikova S.A., Ivanov V.K. Synthesis and Biocompatibility Study of Ceria-Mildronate Nanocomposite in Vitro. *Nanosyst.: Phys. Chem. Math.*, 2022, **13**, P. 96–103.

Submitted 6 September 2023; accepted 11 September 2023

Information about the authors:

Elizaveta A. Zamyatina – Institute of Theoretical and Experimental Biophysics of the Russian Academy of Sciences, Institutskaya str., 3, Pushchino, 142290, Russia; ORCID 0000-0002-1275-565X; sonyoru162@gmail.com

Sergey Yu. Kottsov – Kurnakov Institute of General and Inorganic Chemistry of the Russian Academy of Sciences, Leninskiy prosp., 31, Moscow, 119991, Russia; ORCID 0000-0001-8263-889X; sergey12-17@yandex.ru

Viktoriia A. Anikina – Institute of Theoretical and Experimental Biophysics of the Russian Academy of Sciences, Institutskaya str., 3, Pushchino, 142290, Russia; ORCID 0000-0002-5028-2064; viktoriya.anikina@list.ru

Anton L. Popov – Institute of Theoretical and Experimental Biophysics of the Russian Academy of Sciences, Institutskaya str., 3, Pushchino, 142290, Russia; ORCID 0000-0003-2643-4846; antonpopovleonid@gmail.com

Marina P. Shevelyova – Institute for Biological Instrumentation of the Russian Academy of Sciences, Institutskaya str., 7, Pushchino, 142290, Russia; ORCID 0009-0004-7638-5143; marina.shevelyova@gmail.com

Nelli R. Popova – Institute of Theoretical and Experimental Biophysics of the Russian Academy of Sciences, Institutskaya str., 3, Pushchino, 142290, Russia; ORCID 0000-0002-0982-6349; nellipopovaran@gmail.com

Conflict of interest: the authors declare no conflict of interest.